Integrated Compact Optical Vortex Beam Emitters

Xinlun Cai, Jianwei Wang, Michael Strain, Benjamin Johnson-Morris, Jiangbo Zhu, Erman Engin, Ying-Lung Ho, Marc Sorel, Jeremy O'Brien, Mark Thompson and Siyuan Yu*

We demonstrate ultra-compact vector optical vortex emitters based on the interaction of whispering gallery modes and angular gratings. The devices are fabricated on a silicon-on-insulator substrate. The smallest device is 3.9 micrometers in radius, three orders of magnitude smaller than previously reported devices. The wave-front of the emitted optical beams has been characterised by interference schemes with circularly polarised Gaussian reference beams, confirming that the emitted beams carry well-defined and flexibly reconfigurable orbital angular momentum. As a first step toward photonic integration of optical vortex devices, we further fabricate integrated emitter arrays and demonstrate simultaneous emission of multiple optical vortices. This work enables potential large scale integration of optical vortex emitters on CMOS-compatible silicon chips for wide-ranging future applications.

The discovery that photons in optical vortices - light beams with helical phase fronts and azimuthal component of wave vector - carry orbital angular momentum (OAM) *(1)* has led to high research interests for it potentially wide-ranging applications in optical microscopy (*2*), micromanipulation (*3*), free-space communication (*4*) and quantum information manipulation (*5, 6, 7*). Conventional techniques for generating optical vortices involves passing free space light beams through bulk optic elements including computer generated holograms (*4, 8*), spiral phase plates (*9*), q-plates (*10*), etc.

Photonic integration has been a major propellant for widespread application of photonic technologies due to significant advantages in reliability, miniaturization, and scalability (potential for large scale integration) compared to bulk optics (*11*). Similar benefits can also be gained for OAM optics through integration. In order to facilitate this paradigm change, compact, robust and efficient planar waveguide-based OAM emitters and receivers are critical elements, so that they can be integrated in large numbers, interconnected via waveguides with each other and with lasers and detectors to form photonic integrated circuits (PICs). Recently, a PIC has been reported for multiplexing and de-multiplexing of OAM beams as a means of realizing multi-channel optical communication (*14*). However its large size ($2.5\times1.5mm^2$) and phase-error-sensitive arrayed waveguide structure do not yet support large scale integration.

Here, we report micron-sized silicon-on-insulator (SOI) waveguide OAM emitters able to emit vector optical vortices carrying well defined and quantized OAM. We further demonstrate integrated arrays consisting of such OAM emitters emitting multiple optical vortices simultaneously.

Circular optical resonators, such as micro-rings or micro-disks (*15*), support whispering gallery mode (WGM) modes carrying very high angular momentum. To extract the confined WGM into free space emission, we propose to use angular grating structures embedded into the WGM resonator. An angular grating, such as exemplified in Fig. 2A, is a periodical modulation of refractive index in the azimuthal direction.

The working principle of this idea can be intuitively understood through an analogy with 2^{nd}-order grating structures (Fig. 2B) widely used in straight waveguides as input/output couplers (*16*), which couples the guided wave into a plane wave away from the waveguide. If the

waveguide with grating is curved to form a loop so that the guide wave forms WGMs, by way of Huygens' Principle, the wave-front of the radiated light is also expected to skew in the azimuthal direction and transforms to a helix, suggesting the creation of an OAM-carrying beam (Fig. 2C). This conception has been proven by rigorous theoretical derivation, which shows that a WGM will only emit into a free space beam when the following angular phase matching condition is satisfied (*17*):

$$\nu_{rad} = p - q \tag{1}$$

where p is the azimuthal order of the WGM involved or the number of optical periods around the resonator and q the number of grating elements around the resonator. ν_{rad} is the azimuthal propagation constant (defined as phase shift per unit azimuthal angle) of the radiated beam, which gives rise to orbital angular momentum.

Because the states of the polarization (SOP) of the source WGMs and the angular grating structure are both cylindrically symmetric, the radiated beams should maintain that symmetry and should be cylindrical vector (CV) beams (*18*). In our devices, for quasi-TE WGMs, the radiated near field happens to be predominantly azimuthally polarized (*17*) with its Jones Vector E_{cv} written as (*19, 20*):

$$E_{CV} = \begin{pmatrix} -\sin\theta \\ \cos\theta \end{pmatrix} \exp(i\nu_{rad}\theta) = \begin{pmatrix} -\sin\theta \\ \cos\theta \end{pmatrix} \exp(i(p-q)\theta) \tag{2}$$

where θ is the azimuthal angle (Fig. 1A). With the concept introduced in ref. *20*, we can conclude that the radiated beams are vector vortices with topological Pancharatnam charge of $l=p-q$. The topological Pancharatnam charge, similar to the topological charge in scalar vortices,

is directly related to the OAM of vector vortices - the amount of OAM carried by the radiated beam is $l\hbar$ per photon.

Therefore above concepts give us a very simple yet robust OAM emitter scheme, in which l can only take integer values being determined solely by the difference between integers p and q. Physically Eq.(1) indicates that the angular grating diffracts the light confined in a p-th order WGM (carrying OAM of $p\hbar$ per photon (*17*)) into a free space beam, changing the OAM by an amount of $q\hbar$ per photon in the process. More interestingly, for a fabricated device, q is a structural constant while the value of p can be changed by exciting selected WGMs. Therefore variable OAM can be generated by simply tuning the injected laser wavelength to various cavity resonances, or alternatively tuning cavity resonances with respect to a fixed injection wavelength by changing the refractive index of the cavity material. p can also take negative values corresponding to the opposite WGM propagating direction, which will reverse the sign of l.

To demonstrate the concept of such vortex beam emitters, we have designed and fabricated two types of micro-ring devices (radius R=3.9 μm, q=36 and R=7.5 μm, q=72) on the same SOI chip (*17*). The devices have been designed so that the resonance associated with zero OAM quantum number (l=0) is around the centre of our tunable laser's wavelength range (1470-1580 nm). Fig. 1E-F show the scanning electron microscopy (SEM) images of a device with R=3.9 μm.

Both types of devices have been characterised by launching continuous-wave light from a tunable laser into the access waveguide to excite quasi-TE mode. The near-field intensity of the radiated beam from the devices, with l=0, is annular with a dark centre, as imaged on an infrared camera (Fig. 2A), and indeed is predominantly azimuthally polarized (Fig.2B-E).

The emission spectrum of the device with R=7.5 μm and q=72 is shown in Fig.3A. Each resonance corresponds to a distinctive WGM (*p* value). The emission efficiencies at various resonances are measured to be 5-13%, with stronger emission obtained at longer wavelength side due to the wavelength dependent coupling between the access waveguide and the resonator (*17*).

To characterise the wave-front structure, an interference scheme needs to be used. We observe that the radiated CV vortex beam can be described as the superposition of two orthogonal scalar vortices, as E_{cv} in Eq. (2) can be further decomposed into (*21*):

$$E_{CV} = \frac{i}{2}\begin{pmatrix}1\\-i\end{pmatrix}\exp(i(l+1)\theta) - \frac{i}{2}\begin{pmatrix}1\\i\end{pmatrix}\exp(i(l-1)\theta) \quad (3)$$

which consists of a right-hand circularly polarized (RHCP) beam with topological charge of l+1 and a left-hand circularly polarized (LHCP) beam with topological charge of l-1. This indicates a new way of measuring the value of l: when the radiated beam is made to interfere with a co-propagating circularly polarized reference beam, spiral interference patterns should be produced with the number of arms of either l-1 or l+1, depending on the handedness of the reference beam.

The interference pattern between the radiated beams and co-propagating RHCP or LHCP Gaussian reference beams (Fig 3.B-C) indeed has spiral arms equal to l-1 (RHCP) or l+1 (LHCP), as predicted by Eq.3, and the sign of the topological charge is indicated by the chirality of the pattern. The nine resonances therefore correspond to l=0, ±1, ±2, ±3, ±4. Similar results for the device with R=3.9 μm is given in (17). Moreover, the spiral patterns rotate when the phase of the reference beam is changed continuously (movie S1 and S2). These results manifest unambiguously that the wave-front of the radiated beams is indeed helical with $l=p-q$. Beams

with larger OAM quantum numbers *l* can be generated from the device, however the observable *l* is limited by the tuning range of the tunable laser.

Furthermore, to demonstrate the potential of photonic integration, we fabricated OAM emitter arrays which consist of up to four identical emitters (R=3.9μm, q=36) coupled to the same access waveguide (Fig.4 A). Simultaneous emission of identical vortices has been verified as shown in Fig. 4B and Fig. 4C. The spiral patterns rotate synchronously when the phase of the reference beam is changed (movie S3).

In conclusion, we have demonstrated ultra-compact and reconfigurable OAM emitters based on CMOS-compatible silicon PICs. Optical vortex beams with distinctive OAM are selectively emitted from a very simple and small device, with no need for any fine adjustment of optical phase. While we have already achieve useful emission efficiency of up to 13%, further improved efficiency can be achieved by engineering the coupling ratio between the resonator and the access waveguide to the 'critical coupling' point (*24*), at which all of the input power enters the resonator and most of it radiated provided that the cavity has low intrinsic waveguide loss. As demonstrated by the integrated arrays, such devices can be integrated on silicon wafers in large numbers – potentially up to several thousands - using standard integrated circuit technology, and to form complicated formations.

Such scalable integration potential could open up truly large scale integrated applications opportunities. For example, for quantum and classical information technology applications, it is possible to build OAM quantum communications channels between two chips, each containing the same integrated OAM PICs – one as OAM transmitter and the other as OAM receiver (according to the principle of reciprocity, the device emitting a specific vortex beam will

selectively receive the same beam). While it has been shown that OAM-multiplexing and de-multiplexing can be achieved using PICs (*14*), our device enable rapid switching among OAM states, as semiconductor tunable lasers can already switch wavelengths in nanoseconds (*25*) and silicon micro-rings have been shown to tune at frequencies up to 40 GHz (*26*). Therefore our device provides an approach for integrated OAM switch or modulator. These would allow high capacity communications between chips for data interconnects. Another potential important application area could be micro-manipulation of particles. Due to the demonstrated potential for large scale integration, by selectively lighting groups of these emitters, controllable and reconfigurable drivers can be configured for micro-fluidic and nano-particle manipulation machines, such as lab-on-chip, optical tweezers and optical spanners.

References and Notes

1. L. Allen, M. W. Beijersbergen, R. J. C. Spreeuw, J. P. Woerdman, *Phys. Rev. A* **45**, 8185 (1992).
2. S. Fürhapter, A. Jesacher, S. Bernet, M. Ritsch-Marte, *Opt. Lett.* 30, 1953 (2005).
3. D. G. Grier, *Nature* **424**, 810 (2003).
4. G. Gibson et al., *Opt. Express* **12**, 5448 (2004)
5. A. Mair, A. Vaziri, G. Weihs, A. Zeilinger, Nature 412, 313 (2001).
6. J. Leach et al., *Phys. Rev. Lett.* **92**, 013601 (2004)

7. G. Molina-Terriza, J. P. Torres, L. Torner *Nature Physics* **3**, 305 (2007).

8. N. R. Heckenberg, R. McDuff, C. P. Smith, A. G. White, *Opt. Lett.* **17**, 221 (1992).

9. M. W. Beijersbergen, R. P. C. Coerwinkel, M. Kristensen, J. P. Woerdman, *Opt. Commun.* **112**, 321 (1994).

10. L. Marrucci, C. Manzo, D. Paparo, *Phys. Rev. Lett.* **96**, 163905 (2006).

11. M. Smit, J. van der Tol, M. Hill, *Laser & Photon. Rev.*, **6** 1 (2012).

12. G. Biener, A. Niv, V. Kleiner, E. Hasman, *Opt. Lett.* **27**, 1875 (2002).

13. N. Yu et al., *Science* **334**, 333 (2011).

14. N. K. Fontaine, C. R. Doerr, L. Buhl, in *Optical Fiber Communication Conference*, OSA Technical Digest (Optical Society of America, 2012), paper OTu1I.2.

15. K. J. Vahala, *Nature* 424, 839 (2003).

16. D. Taillaert *et al.*, *Jpn. J. Appl. Phys.* **45** 6071 (2006).

17. Materials and methods are available as supporting material on *Science* Online.

18. R. Dorn, S. Quabis, G. Leuchs, Phys. Rev. Lett. **91**, 233901 (2003).

19. Z. Bomzon, V. Kleiner, E. Hasman, *Opt. Lett.* **26**, 1424 (2001).

20. A. Niv, G. Biener, V. Kleiner, E. Hasman, *Opt. Express* **14**, 4208 (2006).

21. Z. Bomzon, G. Biener, V. Kleiner, E. Hasman, *Opt. Lett.* **27**, 285 (2002).

22. D. S. Weiss et al., *Opt. Lett.* **20**, 1835 (1995).

23. T. J. Kippenberg, S. M. Spillane, K. J. Vahala, *Opt. Lett.* **27**, 1669 (2002).

24. A. Yariv, *Electron. Lett.* **36**, 321 (2000).

25. Y. Yu, R. O'Dowd, *IEEE Photon. Technol. Lett.*, **14**, 1397 (1992).

26. S. Manipatruni, Q. Xu, M. Lipson, *Opt. Express* **15**, 13035 (2007).

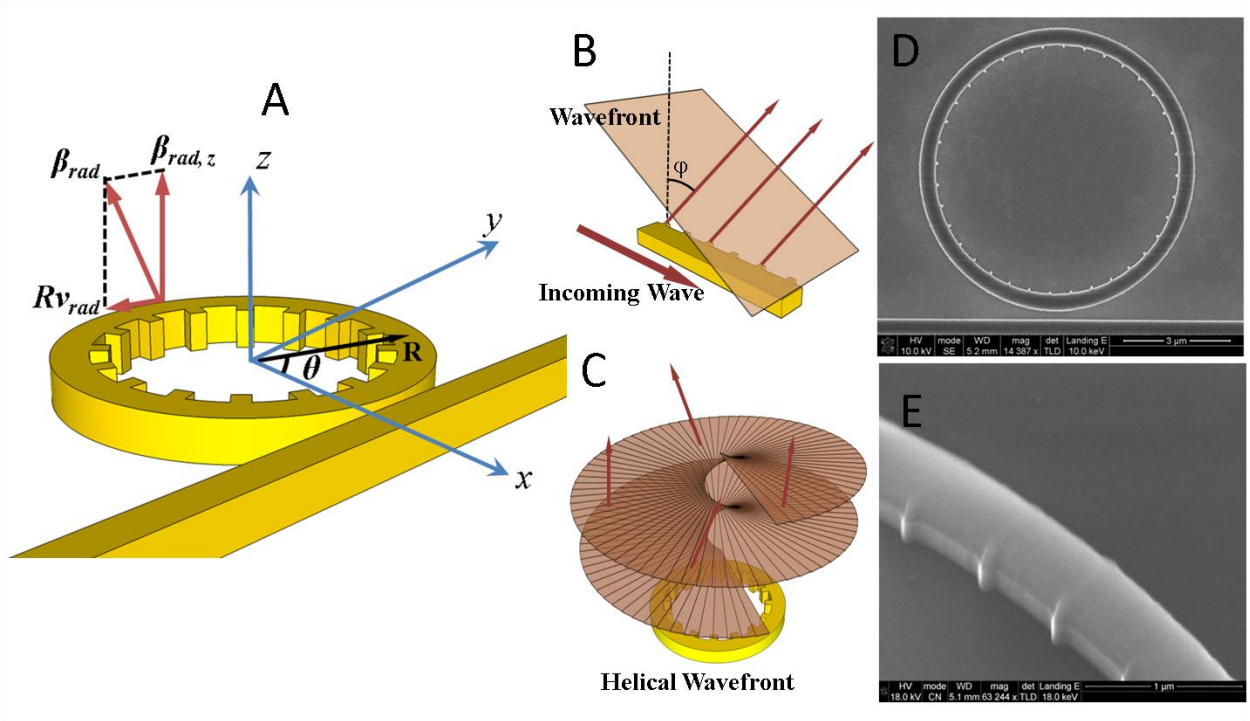

Fig. 1. (**A**) Schematic illustration of the device with angular grating patterned along the inner wall of a micro-ring resonator which is coupled to an access waveguide for optical input. This structure will couple light confined in the WGM into a radiated beam with a paraxial z-component of propagation constant $\beta_{rad,z} = \sqrt{\left(2\pi/\lambda\right)^2 - \left(v_{rad}R\right)^2}$, where λ is the wavelength in free space. The azimuthal component of propagation constant of the radiated beam is Rv_{rad}. (**B**) Schematic illustration of a linear waveguide with gratings. The guided wave is scattered by the grating elements collectively acting as a phased radiation source array, and a significant fraction of power is diverted to a certain direction φ, in which constructive interference occurs. The wave-front of the total radiated field is a plane with titled angle of φ. (**C**)

Schematic illustration of angular grating together with the *helical* wave-front of the radiated beam. (**D**), (**E**) SEM images of a fabricated device (R= 3.9 μm).

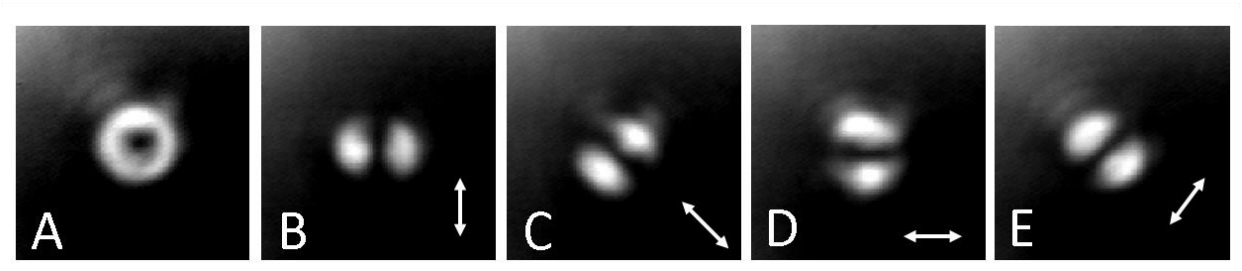

Fig. 2. (**A**) Measured near field intensity distribution of the radiated beam with *l*=0. (**B**)-(**E**) Measured intensity distributions after the polarizer for the directions indicated by the arrows. A two-lobe intensity pattern arranged orthogonal to the polarizer axis is obtained. When the polarizer is rotated, the two-lobe pattern rotates in the same manner, confirming that the radiated beam is a CV beam with azimuthal polarization.

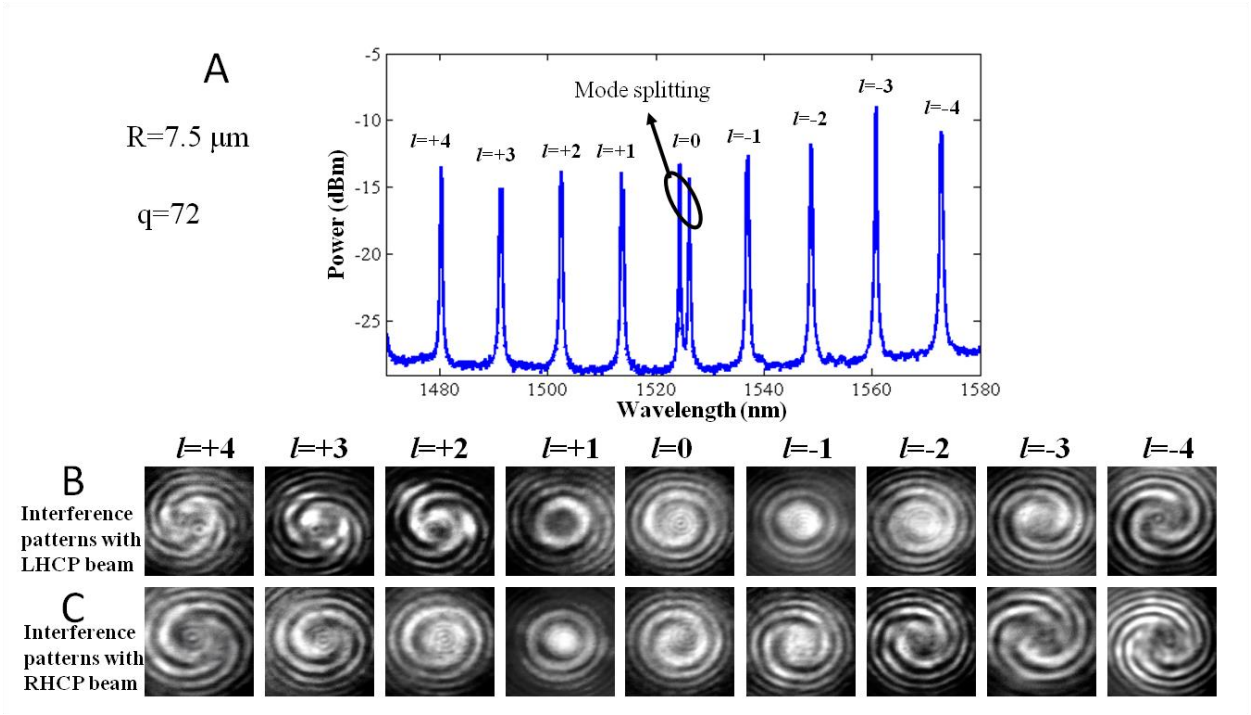

Fig. 3. (**A**) Measured radiation spectrum for a device with R=7.5 μm. The *l*=0 wavelength is about 1525 nm. (**B**)-(**C**). Interference patterns with LHCP and RHCP reference beams. Each pattern in Fig. 3 B has *l*+1 spiral arms while each pattern in Fig. 3 C has *l*-1 spiral arms.

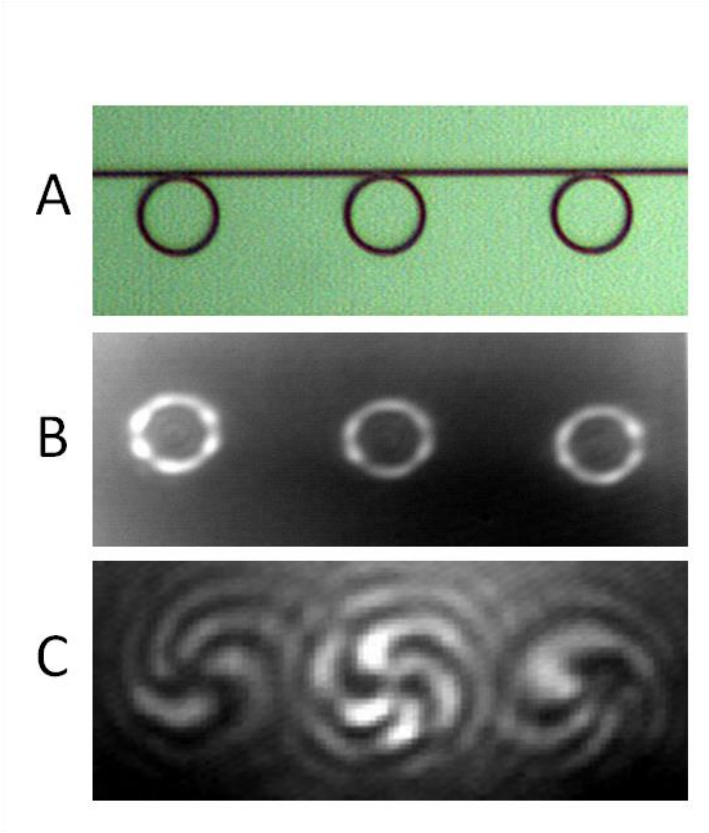

Fig.4 (A) Part of an array consisting of four identical emitters, zoomed-in for clarity. **(B)** Near field intensity patterns emitted from the array. The difference in their brightness is attributed to slight differences in their resonance peaks due to fabrication variations. **(C)** An example of interference pattern between the emitted beams from the array and co-propagating RHCP Gaussian beam. All beams have the same OAM order (l=-3). In (17) all 4 emitters are shown to emit simultaneously.